THE JOURNAL OF PHYSICAL CHEMISTRY A

Article

Imidazo[1,2-*a*]pyrazine-3,6-diones Derived from □-Amino Acids: A Theoretical Mechanistic Study of Their Formation via Pyrolysis and Silica-Catalyzed Process

Flavio F. Contreras-Torres, and Vladimir A. Basiuk

J. Phys. Chem. A, **2006**, 110 (23), 7431-7440 • DOI: 10.1021/jp061331m

More About This Article

Additional resources and features associated with this article are available within the HTML version:

- Supporting Information
- Access to high resolution figures
- Links to articles and content related to this article
- Copyright permission to reproduce figures and/or text from this article

View the Full Text HTML

The Journal of Physical Chemistry A is published by the American Chemical Society.
1155 Sixteenth Street N.W., Washington, DC 20036

Imidazo[1,2-*a*]pyrazine-3,6-diones Derived from α-Amino Acids: A Theoretical Mechanistic Study of Their Formation via Pyrolysis and Silica-Catalyzed Process

Flavio F. Contreras-Torres and Vladimir A. Basiuk*

Instituto de Ciencias Nucleares, Universidad Nacional Autónoma de México, Circuito Exterior C. U., A. Postal 70-543, 04510 México D.F., Mexico

Received: March 2, 2006; In Final Form: April 18, 2006

Imidazo[1,2-*a*]pyrazine-3,6-diones are unusual compounds composed of three α-amino acid fragments. These bicyclic amidines (BCAs) form under high temperatures or with the use of strong dehydrating reagents. We gave insight into the mechanisms of BCA formation via gas-phase pyrolytic and silica-catalyzed reactions of glycine (Gly) and α-aminoisobutyric acid (AIB) with related diketopiperazines (DKPs), using quantum chemical calculations. The entire process requires four steps: (1) O-acylation of DKP with free or silica-bonded amino acid, (2) acyl transfer from the oxygen to the nitrogen atom, (3) intramolecular condensation of the *N*-acyl DKP into a cyclol, and (4) elimination of water. To study step (1) at silica surface (modeled by $H_7Si_8O_{12}$−OH cluster), we employed two-level ONIOM calculations (AM1:UFF, B3LYP/3-21G:UFF and B3LYP/6-31G(d):UFF); all gas-phase reactions were studied at the AM1, B3LYP/3-21G and B3LYP/6-31G(d) levels. The catalytic effect of silica was observed for both Gly and AIB: the activation energy in the O-acylation at the surface was lower by more than 9 kcal mol^{-1} as compared to the gas-phase process. Contrary to the exothermic O-acylation, the gas-phase transfer reaction (step 2) was exothermic in both cases, but more favorable for Gly. The cyclocondensation of N-acylated DKPs into BCAs (steps 3 and 4) is endothermic for Gly and exothermic for AIB.

1. Introduction

The importance of amino acid, peptide and protein chemistry for all Terrestrial life made this research area one of the best-explored areas of contemporary chemistry. The infinite number of combinations of ca. 20 α-amino acids, producing the well-known bioorganic compounds, contemplates two general ways of interconnecting amino acid residues, namely in the form of linear and cyclic peptide chains. This fact is so natural and trivial that one can hardly think of other existing covalent patterns to unite a few amino acid fragments.

Nevertheless, such patterns do exist, and their unusual formation mechanisms represent a field that is necessary to explore and understand. In particular, an important class of bicyclic compounds called imidazo[1,2-*a*]pyrazines[1] includes several amidines derived from α-amino acids. Mechanisms of their formation in different reaction systems are not completely understood, although chemical synthesis of the few known derivatives was reported long ago. By using harsh condensing agents $PtCl_5$ or $SOCl_2$, were synthesized bicyclic and tricyclic amidine-type derivatives (BCA and TCA, respectively; Chart 1) of α-aminoisobutic acid (AIB; also called α-methylalanine), first by Jones et al.[2,3] and then by Titlestad and Ali.[4−7] Both groups employed linear peptides of AIB as starting materials. The former group described a method for BCA synthesis from AIB−AIB−AIB tripeptide. In addition to that, the latter group managed also to synthesize TCA using related tetra or pentapeptides instead. We would like to emphasize that these approaches have to use harsh condensing agents to be successful, whereas it is well-known that peptide formation in an aqueous solvent environment without condensing reagents is unfavorable both kinetically and thermodynamically.[8] A high sensitivity to hydrolysis and a high activation energy to cross the transition states can inhibit the product formation. Because the amidines are composed of amino acid structural units, one can think that BCAs and TCAs can form through a mechanism where intermolecular cyclocondensation of the amino acid monomers or their activated derivatives would play a crucial role. Then, the most critical step must be the formation of dipeptides, followed by their dehydrocyclization into cyclic dipeptides commonly called piperazine-2,5-diones or diketopiperazines (DKPs). However, the condensation processes are hardly possible under homogeneous conditions, and heterogeneous catalysis on mineral surfaces such as clays, alumina and silica turned out to be a better practical way to explain the peptide chain elongation under moderate temperature conditions.[9]

CHART 1: Bicyclic (BCA, Left) and Tricyclic (TCA, Right) Amidines Derived from α-Amino Acids[a]

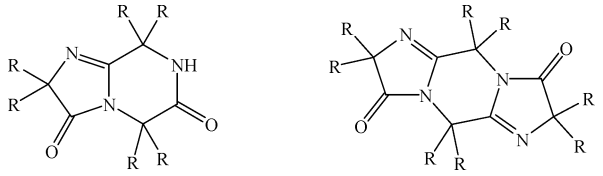

[a] Systematic names: 2,3,5,6,7,8-hexahydroimidazo[1,2-*a*]pyrazine-3,6-dione and 2,3,5,7,8,10-hexahydrodiimidazo[1,2-*a*;1′,2′-*d*]pyrazine-3,8-dione, respectively.

The explanation of possible mechanisms of amino acid condensation and peptide chain elongation has a paramount importance for prebiotic chemistry and the problem of the origin of Life. During past decades, a number of related prebiotic scenaria were proposed. For example, due to the abundance of metal cations (e.g., Na, Ca, Al, and Fe) in clays and seawater,

* Author for correspondence: Phone: (52) 55 56 22 47 39, ext. 224. Fax: (52) 55 56 16 22 33. E-mail: basiuk@nucleares.unam.mx.

10.1021/jp061331m CCC: $33.50
Published on Web 05/18/2006

the salt-induced peptide formation reaction was suggested to be the simplest and most universal mechanism to produce peptides from amino acid building blocks.[10] Nevertheless, most studies in this area[11−30] focus on the role of catalytically active inorganic oxide surfaces. In turn, pure cation-free silica and alumina became the most commonly used models of clays and other complex minerals, where the role of surface silicon and aluminum atoms in the process of amino acids activation became another specific problem. In particular, silanol SiOH and aluminol AlOH groups were proposed as the surface active sites capable of reacting with amino acids to produce ester-type bonds X−O−R (where X = Si or Al; R = amino acid acyl).[29] These surface compounds are believed (by some authors) to play the role of "activated intermediates" in the heterogeneous catalysis of polycondensation of amino acids into peptides.[30] The incorporation of dehydration catalysts such as silica into the reaction system, might influence the entire process in three ways: (1) it offers a surface where the amino acids are concentrated through adsorption and chemically linked, (2) the catalytic process can help to reduce the height of activation barrier, and (3) it can generate dehydration products such as DKPs, which are capable per se of acting as acylation agents for further peptide chain elongation.

We also attempted to give an insight into the mechanisms of amino acids interaction with silica and alumina surfaces with an emphasis on prebiotic chemistry aspects.[24−28] The ester-type "activated intermediates" were found indeed chemically active only on the silica surface, where the composition of final condensation products varied depending on the degree of surface dehydration. The formation of linear peptides was more favorable when at least small amounts of water were available, whereas DKPs were major products on silica with a higher degree of dehydration, in particular upon amino acid sublimation in the presence of silica at ca. 200 °C.[24] Furthermore, the DKP yields were high enough to allow for a novel method of their preparation to be designed,[25,26] namely for DKPs derived for glycine, alanine, valine, leucine and proline. The products, however, contained some colored impurities, whose chloroform extraction and preliminary analysis by mass spectrometry revealed the presence of BCAs and TCAs (except for proline) at a percent level.[28] All those results indicated that our knowledge of the amino acid chemistry under harsh temperature conditions remains very incomplete.

More recently, by using the hyphenated technique of gas chromatography−Fourier transform infrared spectroscopy−mass spectrometry (GC−FTIR−MS) we found that the same BCAs and TCAs can also be detected in the experiments on catalyst-free amino acid pyrolysis at 500 °C.[31,32] Obviously, the pyrolysis is not an appropriate method to generate the amidines, because it simultaneously produces a large number of simple decomposition products and thus makes separation and purification of BCAs and especially TCAs extremely complicated or even impossible.[33,34] On the other hand, introducing silica gel into the reaction system and reducing the amino acid sublimation temperature to 200−300 °C allowed us to afford the BCA yields of 1−10% (according to rough estimates).[35] The bicyclic amidine derived from AIB was successfully separated from the condensation products (mainly DKP) obtained in this way, and its crystal structure was characterized by X-ray diffraction.[36]

Thus, the thermochemical process with or without catalyst, which was apparently very common under prebiotic conditions, is able to form the amidines along with DKPs in appreciable amounts. The suggested two mechanisms of BCA formation[28,31b] are shown in Scheme 1, where the amidine (**3**) can form through

SCHEME 1

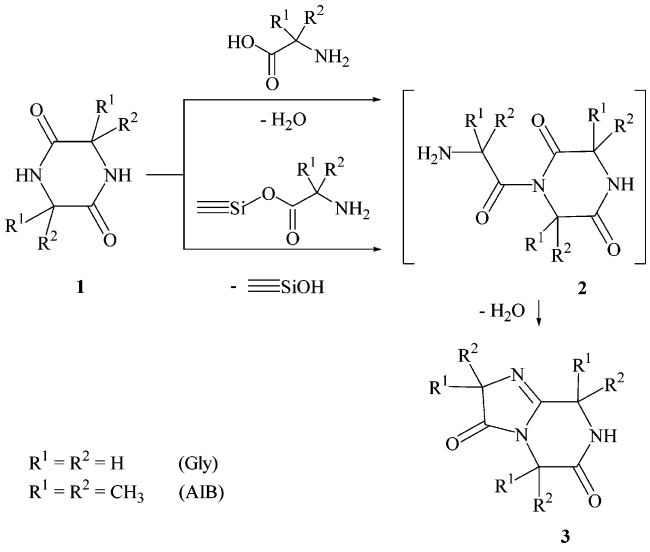

the N-acylation of monocyclic DKP (**1**) either with a single amino acid molecule (e.g., under gas-phase pyrolytic conditions; above) or with amino acid covalently linked to silica surface through the ester-type bond (below). We believe that the N-acylated DKP (**2**) is an intermediate in both cases. No experimental evidences have been afforded so far, and under these circumstances, theoretical mechanistic studies would be very helpful. Quantum chemical calculations already helped to give some insight into the prebiotic amino acid chemistry at surfaces.[37−39] The real catalytic system of interest are very large and thus computationally very demanding, limiting the researches to relatively small model systems. For example, Ugliengo et al.[37] studied the amide bond formation between glycine and ammonia to simulate the formation of Gly-Gly dipeptide. Another necessary and helpful simplification is the choice of small Si-containing clusters to simulate silica surface.[37−44]

The goal of the present theoretical study was to compare the two routes of BCA formation (Scheme 1) for two representative amino acids, Gly and AIB. The choice of amino acids allows for taking into account the effect of α-substituent. Because the above goal forced us to keep the three amino acid residues intact, without any simplification, the only way to reduce the computation cost for the silica-catalyzed process was to choose small surface clusters and to employ a hybrid quantum mechanical/molecular mechanical technique.

2. Computational Details

Because amorphous silica consists of a network of tetrahedric SiO_4 building blocks with a random orientation, a serious computational problem appears when one wants to optimize its geometry. In resistance to tetrahedric rigid angles O−Si−O, some Si−O−Si angles can change without substantial energetic effects from 130° to their linealization with as small a barrier as 0.4 kcal mol^{-1}.[40] Due to the high flexibility of Si−O−Si angles, it is possible to model a silica surface with a small cage where the degrees of freedom related to Si−O rotations are eliminated. In this way, the catalytic SiOH sites can be adequately represented, along with a considerable saving in the calculation cost. Our selection of the silica-modeling cluster was based on the previous studies by Sauer et al.[40] and Ugliengo's group.[41−44] In particular, Sauer et al.[40] proposed a cage-like model belonging to the class of hydridosilasesquioxanes, which

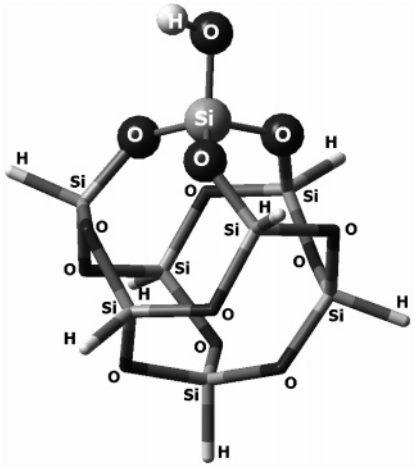

Figure 1. $H_7Si_8O_{12}$−OH cluster employed for the ONIOM2 calculations of silica-catalyzed reactions. The atoms represented by ball-and-stick model (O_3Si−OH) were treated with quantum mechanics; the remaining atoms represented by tube model were treated with UFF molecular mechanics.

carries one hydroxyl group to represent the isolated silanol group at the silica surface. The suitability of the $H_7Si_8O_{12}$−OH cluster was further proved by Ugliengo's group in terms of vibrational features,[41] isotropic NMR chemical shielding,[42] and the interaction with NH_3 molecule.[43] In addition to that, hybrid computation schemes (e.g., ONIOM), which do not require a full ab initio treatment, can be adopted to model very large fragments of siliceous materials. For example, the physisorption of NH_3 molecule at the isolated SiOH group was studied by means of ONIOM2 technique using the octahydrosilasesquioxane cluster, where only the O_3Si−OH fragment was selected for the high-level description.[44] We employed the same $H_7Si_8O_{12}$−OH cluster (Figure 1) and the same high-level fragment for the ONIOM2 calculations of the silica-catalyzed acylation of DKPs derived from Gly and AIB. Along with the O_3Si−OH fragment, the high level also included the full organic part, namely the corresponding DKP and the ester-type surface derivative of Gly or AIB.

The Gaussian 03W suite of programs[45] was used for all calculations. Stationary point geometries for the gas-phase reactions were optimized at a single theoretical level, with a semiempirical (pre-optimization) or density functional theory (DFT) method. For the silica-catalyzed process, we employed a hybrid two-level quantum mechanical/molecular mechanical (QM/MM) technique to take advantage of the division of the system into a critical QM region and a noncritical MM region. The ONIOM2 scheme[46] implemented in Gaussian 03W uses microiterations[47] to optimize the MM region for each optimization step in the QM region. The regular Berny algorithm using nonredundant internal coordinates was used for the high-level optimizations. The low level comprising a major part of the cluster modeling silica, does not participate in the formation and rupture of chemical bonds; it served to simulate only steric influence of the surface, and was described with the UFF force field.[48] The high level was treated with AM1 or DFT. The DFT calculations were performed with Becke's three-parameter hybrid functional[49] and Lee, Yang and Parr's (LYP)[50] correlation functional. B3LYP method was used in conjunction with the 3-21G[51] and 6-31G(d)[52] basis sets. The stationary point geometries were fully optimized and characterized as minima (no imaginary frequencies) or first-order saddle points (one imaginary frequency) by calculations of vibration frequencies. Naturally, studies of the AIB systems turned to be much more computationally demanding due to the presence of six CH_3 groups and their high rotational freedom. Only B3LYP/6-31G(d) SCF energies and geometries are discussed in the text; AM1 and B3LYP/3-21G SCF energies are specified in Tables 1 and 2 for comparison.

TABLE 1: Energies (in kcal mol^{-1}) Relative to the Reactant Level for Reaction Complexes (RCs), Transition States (TSs) and Products (Ps) for the Formation of BCA 2,3,5,6,7,8-Hexahydroimidazo[1,2-*a*]pyrazine-3,6-dione (3; R = H) from One Gly Molecule and One Molecule of Related DKP[a]

	AM1		B3LYP/3-21G		B3LYP/6-31G(d)	
	gas phase	SiO_2	gas phase	SiO_2	gas phase	SiO_2
RC1	−4.9	1.8	−21.0	−9.8	−8.7	1.7
TS1	53.8	76.0	20.8	21.4	38.2	39.5
P1	15.6	35.0	−15.3	13.4	17.1	20.4
RC2	0.0		0.0		0.0	
TS2	52.5		12.9		18.9	
P2	−9.6		−23.4		−16.3	
RC3	0.0		0.0		0.0	
TS3	65.5		34.1		41.4	
P3═RC4	12.6		1.3		3.0	
TS4	78.8		46.9		50.8	
P4	13.7		14.4		6.2	

[a] Energies for the gas-phase reaction were calculated at AM1, B3LYP/3-21G and B3LYP/6-31G(d) levels of theory. Energies for the silica-catalyzed DKP acylation with Gly surface ester were calculated at ONIOM2 AM1:UFF, B3LYP/3-21G:UFF and B3LYP/6-31G(d):UFF levels of theory. For the very first step in the gas-phase and silica-catalyzed processes, which is a bimolecular reaction, relative energies were calculated according to the following formula: $\Delta E_x = E_x - (E_A + E_{DKP})$ where E is absolute energy; x is RC1, TS1 or P1; A is Gly or its surface ester. All the further chemical transformations are monomolecular reactions, and therefore relative energies were calculated with respect to the level of the corresponding reaction complexes RCi according to the following formula: $\Delta E_x = E_x - E_{RCi}$ where E is absolute energy; x is TS or P; $i = 2,3$.

TABLE 2: Energies (in kcal mol^{-1}) Relative to the Reactant Level for Reaction Complexes (RCs), Transition States (TSs) and Products (Ps) for the Formation of BCA 2,2,5,5,8,8-Hexamethyl-2,3,5,6,7,8-hexahydroimidazo[1,2-*a*]-pyrazine-3,6-dione (3; R = CH_3) from One AIB Molecule and One Molecule of Related DKP

	AM1		B3LYP/3-21G		B3LYP/6-31G(d)	
	gas phase	SiO_2	gas phase	SiO_2	gas phase	SiO_2
RC1	−4.8	4.8	−21.0	−14.1	−10.8	−7.0
TS1	55.9	71.9	15.8	8.8	36.5	30.7
P1	18.2	29.6	−16.3	1.5	19.8	11.7
RC2	0.0		0.0		0.0	
TS2	51.5		19.6		24.1	
P2	−2.8		−11.2		−4.4	
RC3	0.0		0.0		0.0	
TS3	57.8		22.0		31.5	
P3═RC4	7.7		−7.4		−2.9	
TS4	73.1		36.9		41.6	
P4	6.3		1.2		−7.5	

3. Results and Discussions

As mentioned in the previous section, the high level was treated with AM1, B3LYP/3-21G and B3LYP/6-31G(d), and UFF force field was used for the low-level description (that is, AM1:UFF, B3LYP/3-21G:UFF and B3LYP/6-31G(d):UFF, respectively). Similarly, single-level calculations with the AM1, B3LYP/3-21G and B3LYP/6-31G(d) methods were used to study the gas-phase steps of BCA formation. The calculated energies (in kcal mol^{-1}; relative to reactant level) of optimized stationary point geometries for the Gly and AIB reactions are

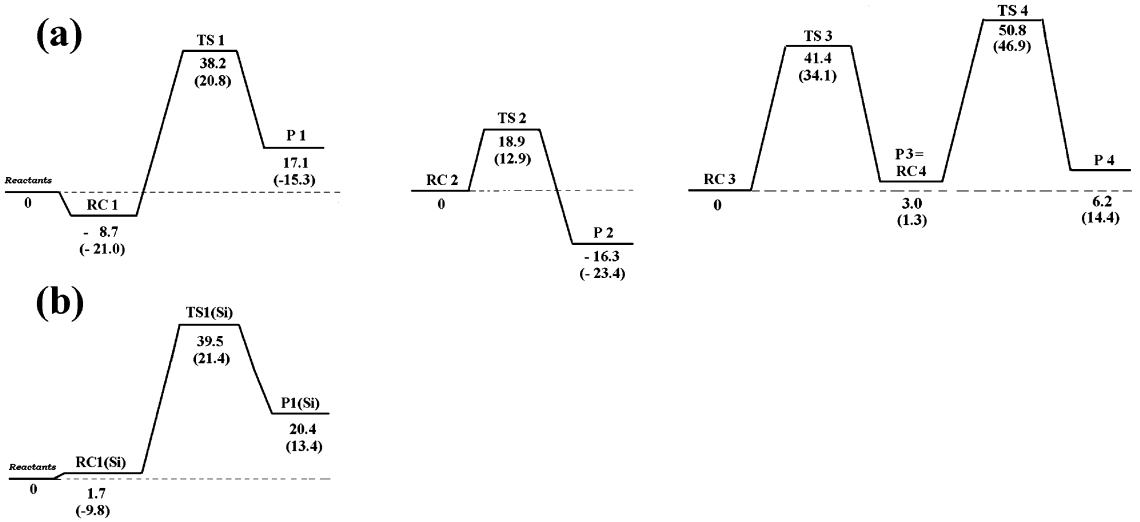

Figure 2. Relative energy profiles (energies in kcal mol^{-1}) for the formation of BCA derived from Gly: (a) the gas-phase reaction sequence, computed at the B3LYP/6-31G(d) and B3LYP/3-21G (upper and lower values, respectively); (b) the silica-catalyzed DKP acylation with Gly surface ester, computed at the ONIOM2 B3LYP/6-31G(d):UFF and B3LYP/3-21G:UFF (upper and lower values, respectively). Optimized structures for the stationary points are shown in Figures 3 and 4.

specified in Tables 1 and 2, respectively. Figure 2 shows energy profiles for the Gly reactions, and Figures 3 and 4 represent details of all the stationary point geometries (reaction complexes, RCs, transition states, TSs, and products, Ps) found for this reaction. Analogous data for the AIB reaction sequences are shown in Figures 5−7. For the silica-catalyzed processes, alternative to DKP acylation with amino acid molecule is the acylation with ester-type "activated intermediate". Once the acylated DKP formed at the surface, it can desorb, and further dehydrocyclization into BCA can proceed in the gas phase. (Strictly speaking, we cannot exclude that the latter can occur on silica surface as well. However, we believe that the critical step is DKP acylation, which therefore was the only one considered in detail in the present study.)

It becomes evident from Figures 2−7 that the entire reaction sequences include four major transition states. Hydrogen bonding plays an important role for all the stationary points. For the first reaction complexes (RC1s) we analyzed not only interatomic distances related to the hydrogen bonds and bonding energies but also stretching vibration frequencies of X−H bonds of the proton-donor molecules. In Gly RC1 (gas-phase reaction; Figure 3), the carboxylic group is coordinated to the peptide bond of DKP, where the H-bonded groups form a six-membered ring. The resulting OH···O separation is 1.777 Å, whereas NH···O is notably longer, 2.163 Å. Besides that, the carboxylic O−H bond and N−H of DKP slightly increase in length, by 0.022 and 0.004 Å, respectively. Figure 8 shows electrostatic potential distribution for Gly and related DKP molecules, where negative potential is predominantly located around lone electron pairs of the oxygen atoms in C═O groups, thus explaining the H-bonding pattern observed. The bonding energy for this reaction complex is 8.7 kcal mol^{-1} as calculated with B3LYP/6-31G(d) (Table 1 and Figure 2). For the AIB reaction, the H-bond separations in RC1 are insignificantly different, namely OH···O of 1.759 Å and NH···O of 2.221 Å (Figure 6). As a whole, AIB RC1 geometry is very similar to the one for Gly RC1, but at the same time more stable, by 2.1 kcal mol^{-1} (Table 2 and Figure 5). As regards harmonic vibration frequencies (nonscaled, calculated at the B3LYP/6-31G(d) theoretical level), the normal stretching modes O−H and N−H for Gly RC1 were at 3282 and 3534 cm^{-1}, respectively; for AIB RC1, they were at 3250 and 3515 cm^{-1}, respectively, that is slightly lower than those for Gly RC1. Recently we studied the basis set effect in B3LYP calculations of harmonic frequencies for Gly derived BCAs and TCAs, in particular for 2,3,5,6,7,8-hexahydroimidazo-[1,2−*a*]pyrazine-3,6-dione,[53] where no convincing improvement was found beyond 6-31G(d) basis set. For the latter case, the N−H stretching mode was observed at 3598 cm^{-1}. Therefore, H-bonding in Gly RC1 decreases the ν_{NH} frequency by 64 cm^{-1}.

Instead of the free Gly and AIB molecules in the gas-phase process, as the acylating reactant for the silica-catalyzed process, we considered Gly and AIB amino acids chemically bound to silica-modeling cluster $H_7Si_8O_{12}$−OH[40−44] through an ester-type linkage. The linkage can be formed by the condensation of the COOH group of the amino acid and the SiOH group of the surface releasing one water molecule. According to our previous results, this process is favorable under anhydrous conditions and elevated temperatures.[24,27] The ester-type linkage can be identified in IR spectra due to the $\nu_{C=O}$ band at 1750−1760 cm^{-1}.[24,27,29] For several decades, it was believed to be an "activated intermediate" in the silica-catalyzed intermolecular condensation of amino acids.[20−22,24−28,30] On the other hand, recent quantum chemical calculations by Ugliengo's group[39] did not confirm the enhanced reactivity of this linkage. We hoped to provide an additional insight for our particular type of surface reactions.

Like the gas-phase Gly RC1 (Figure 3), its silica-bound counterpart Gly RC1(Si) is stabilized by two H-bonds (Figure 4). In this case, both bridges are NH···O, with the separations of 2.232 and 2.134 Å. Both bridges are NH···O (2.176 and 2.052 Å) for AIB RC1(Si) as well. However, the presence of bulky geminal CH_3 groups in AIB DKP does not allow its NH group to approach the oxygen atom of the Si−O−C linkage. Instead, the NH group forms a H-bond with one of the siloxane oxygen atoms of the $H_7Si_8O_{12}$−OH cluster. Despite the above steric obstruction, the formation energy for AIB RC1(Si) is 8.7 kcal mol^{-1} lower than that for Gly RC1(Si), as calculated at the ONIOM2 B3LYP/6-31G(d):UFF level of theory. Although the energetic stability for both RC1(Si) complexes is lower as compared to their gas-phase counterparts (by 10.4 and 3.8 kcal mol^{-1} for Gly and AIB, respectively), the catalytic effect of silica can be seen by comparing reaction enthalpies ΔH, where all the acylation reactions turn to be highly endothermic. For Gly, they are 25.8 and 18.7 kcal mol^{-1} for the gas-phase and

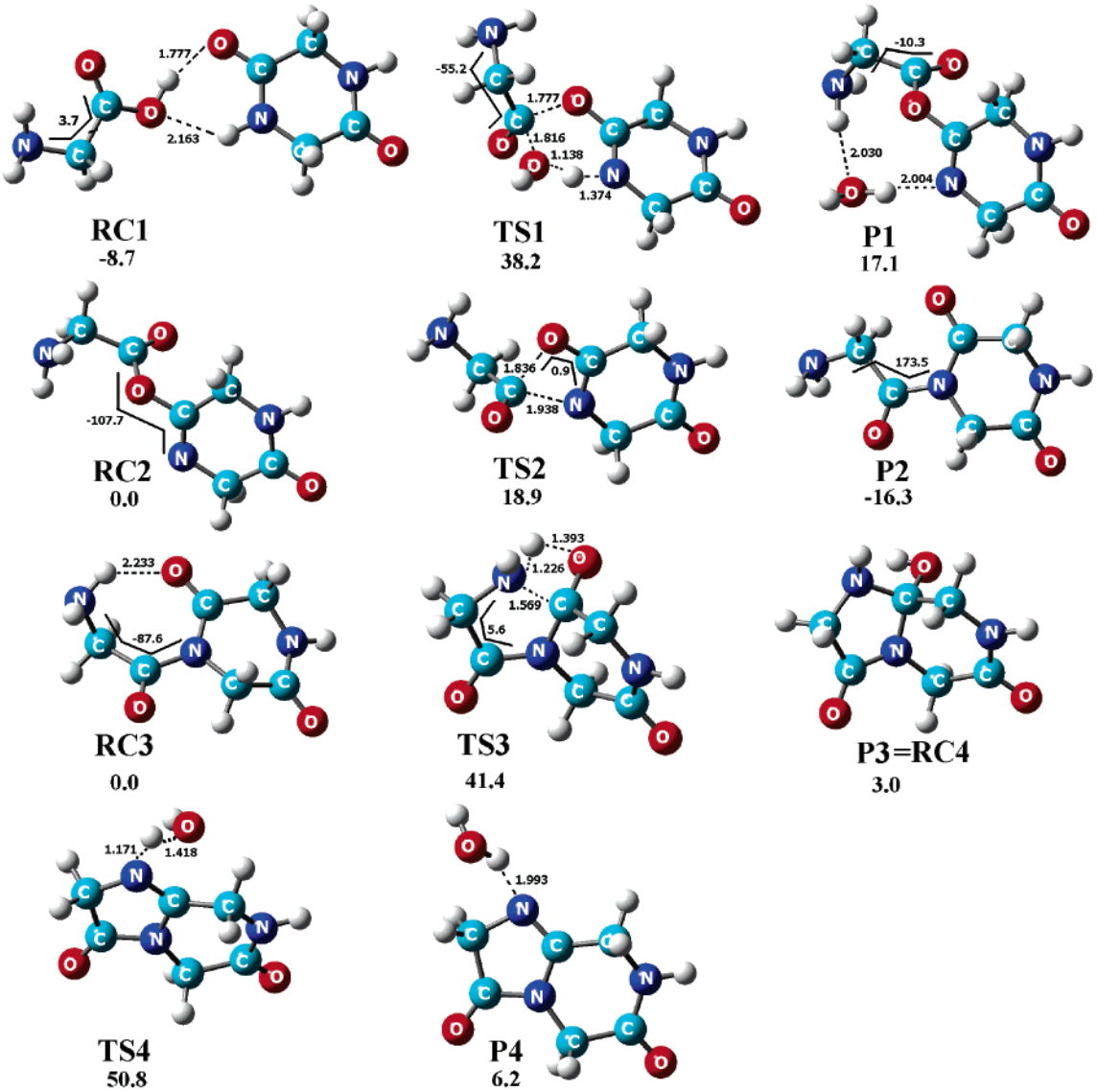

Figure 3. Optimized geometries for reaction complexes (RCs), transition states (TSs) and products (Ps) for the gas-phase formation of BCA derived from Gly, computed at the B3LYP/6-31G(d) level of theory. Selected interatomic distances (in angstroms), dihedral angles (in degrees) and SCF energies (in kcal mol^{-1}) are specified.

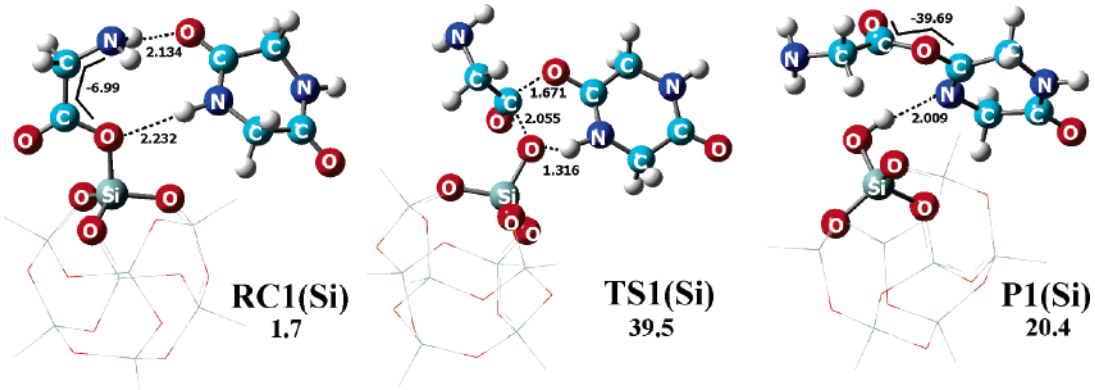

Figure 4. Optimized geometries for reaction complex (RC1(Si)), transition state (TS1(Si)) and product (P1(Si)) for the silica-catalyzed DKP acylation with Gly surface ester, computed at the ONIOM2 B3LYP/6-31G(d):UFF level of theory. The atoms represented by ball-and-stick models were treated with B3LYP/6-31G(d) quantum mechanics; the atoms represented by wire frame models were treated with UFF molecular mechanics. Selected interatomic distances (in angstroms), dihedral angles (in degrees) and SCF energies (in kcal mol^{-1}) are specified.

silica-catalyzed reactions, respectively, and for AIB, they are 30.6 and 18.7 kcal mol^{-1} for the gas-phase and surface reactions, respectively (all values relative to the level of RC1s). These values show the importance of hydrogen bonding for the stabilization of reaction complexes, which is more favorable under homogeneous conditions.

As another criterion of reactivity in the systems studied, the activation energies ΔE_a (relative to the level of RC1s) were

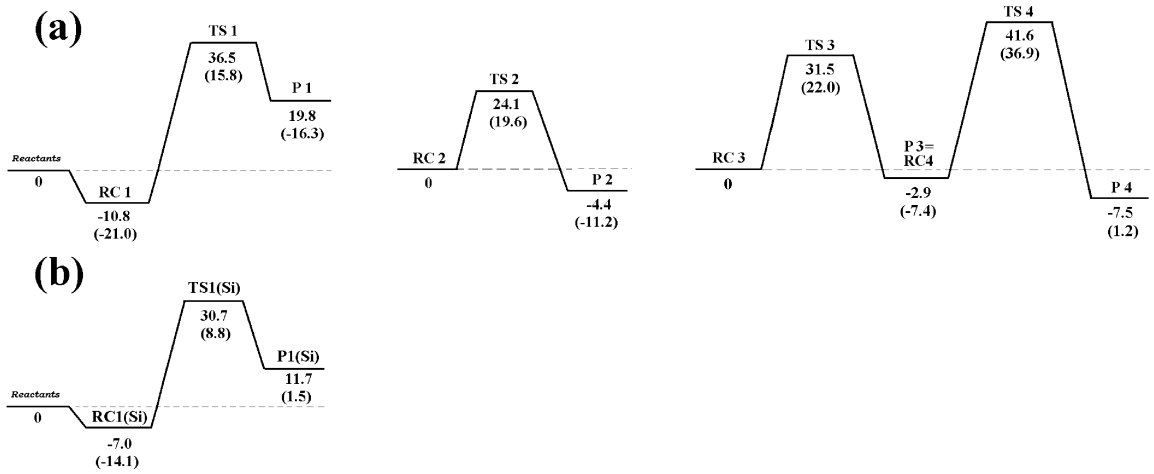

Figure 5. Relative energy profiles (energies in kcal mol^{-1}) for the formation of BCA derived from AIB: (a) the gas-phase reaction sequence, computed at the B3LYP/6-31G(d) and B3LYP/3-21G (upper and lower values, respectively); (b) the silica-catalyzed DKP acylation with AIB surface ester, computed at the ONIOM2 B3LYP/6-31G(d):UFF and B3LYP/3-21G:UFF (upper and lower values, respectively). Optimized structures for the stationary points are shown in Figures 6 and 7.

compared. For Gly, their values are 37.8 and 46.9 kcal mol^{-1} for the surface and gas-phase reactions, respectively; for AIB, the corresponding values are 37.7 and 47.3 kcal mol^{-1}. Thus, here the catalytic effect of silica is clearly seen as well, because it reduces the activation energy by more than 9 kcal mol^{-1} in both cases. The above data were calculated at the highest level employed, that is, with B3LYP/6-31G(d). For the lower-theory calculations, i.e., with AM1 and B3LYP/3-21G (Tables 1 and 2), the trend is similar, so that these methods can apparently be validated for the use with more extended molecular systems of analogous chemical nature.

We calculated the Gibbs free energies (relative to the level of reactants) for stationary points in the gas-phase and silica-catalyzed O-acylation reactions. The values calculated at 298 K (ΔG_{298}) are summarized in Table 3. One can see that all the O-acylation products are thermodynamically unstable, with variable ΔG_{298} values of 25.2−34.1 kcal mol^{-1}. A fraction of 13 kcal mol^{-1} on average is introduced by entropic effects in each system. For the gas-phase reaction between Gly and DKP, the reaction barrier is $\Delta G^{\ddagger} = 49.2$ kcal mol^{-1}, which is 2.1 kcal mol^{-1} lower than the barrier computed for the silica-catalyzed process. On the other hand, the catalytic effect of silica can be seen for AIB, although the activation barrier for the silica-catalyzed proccess is only 3.3 kcal mol^{-1} lower as compared to the gas-phase process. On the basis of the transition state theory, the reaction rates were calculated as well, by taking the reactants as the reference state and using the concentration $c^{\circ} = 1$. In the case of Gly, we found that the silica-catalyzed reaction at 298 K has a rate of 1.54×10^{-25} s^{-1} L mol^{-1}, which means that this reaction would not proceed at room temperature. However, when recalculated for the average temperature of 473 K commonly used in our previous experiments,[24−28,31,32,35,36] this rate dramatically increases to 3.22×10^{-10} s^{-1} L mol^{-1}. For AIB, the reaction rates behave similarly, giving the value of 2.46×10^{-10} s^{-1} L mol^{-1} for 298 K and 4.19×10^{-07} s^{-1} L mol^{-1} for 473 K, which is the highest rate for the reactions considered here.

As was logical to expect, the search for transition states was the most challenging task in our calculations (rational function optimization, RFO, by Simons et al.[54] was employed). It dramatically complicates when one has only a limited (or incorrect at all) idea on the transition state structure. We used TS and QST3 search methods. In cases when transition states were found by the TS method, they were confirmed by QST3 calculations, after slightly distorting the transition state geometry found previously. All the transition states found exhibited one imaginary frequency in their vibration spectra. In particular, the calculated absolute values for imaginary frequencies were 717 (Gly TS1), 634 (Gly TS1(Si)), 855 (AIB TS1) and 278 cm^{-1} (AIB TS1(Si)) at the B3LYP/6-31G(d) theoretical level.

Although the piperazine rings in Gly and AIB DKPs undergo no substantial distortion, the rotation around the C−C bond in free and silica-bound amino acids has to be very considerable to allow for the quaternization of carbon atoms of C═O groups. In Gly TS1 (Figure 3), this C atom approaches the carbonyl oxygen ($O_{carbonyl}$) atom of DKP by 1.777 Å; in Gly TS1(Si) (Figure 4), this distance becomes even shorter, 1.671 Å. Simultaneously, the O atoms of OH ($O_{hydroxyl}$) and Si−O−C coordinate to the amide hydrogen (H_{amide}) atoms of Gly DKP with the O···H distances of 1.138 and 1.316 Å, respectively. AIB TS1 and TS1(Si) geometries exhibit similar features (Figures 6 and 7), with (O)C···O═C distances of 1.708 Å in AIB TS1 and of 1.674 Å in AIB TS1(Si); the oxygen atoms of OH and Si−O−C coordinate to H_{amide} atoms of AIB DKP with O···H distances of 1.167 and 1.428 Å, respectively. The increased N−H bond length in DKPs (e.g., to 1.374 Å in Gly TS1 and 1.323 Å in AIB TS1), preceding the loss of a water molecule, is compensated by shortening of the N−C(═O) bonds to the values typical for double bonds (1.289 and 1.294 Å, respectively).

As mentioned above, the Gly acylation reactions in the gas phase and on silica are endothermic by 25.8 and 18.7 kcal mol^{-1}, respectively (values relative to the level of RC1s). For AIB, they are endothermic by 30.6 and 18.7 kcal mol^{-1}, respectively. TS1 and TS1(Si) structures indicate that the reaction mechanism includes an attack of the carbonyl C atoms ($C_{carbonyl}$) of amino acid or surface ester on the amide oxygen atoms (O_{amide}) in DKPs, along with transfer of the amide protons to the hydroxylic or silanol O atoms, respectively. Simultaneous cleavage of the carboxylic HO−C(═O) and ester SiO−C(═O) bonds produces P1 and P1(Si), respectively. Due to the proximity to SiO, the $C_{carbonyl}$ atom in surface esters is more acidic (as a Lewis acid) than in the corresponding free amino acids. The HO−C(═O) and SiO−C(═O) bond strength along with electrophilic/nucleophilic characteristics of the atoms involved in the formation of new covalent bonds can be adequate descriptors for the reaction mechanisms and thermodynamics. For the O-acylation reactions under study, we employed the following

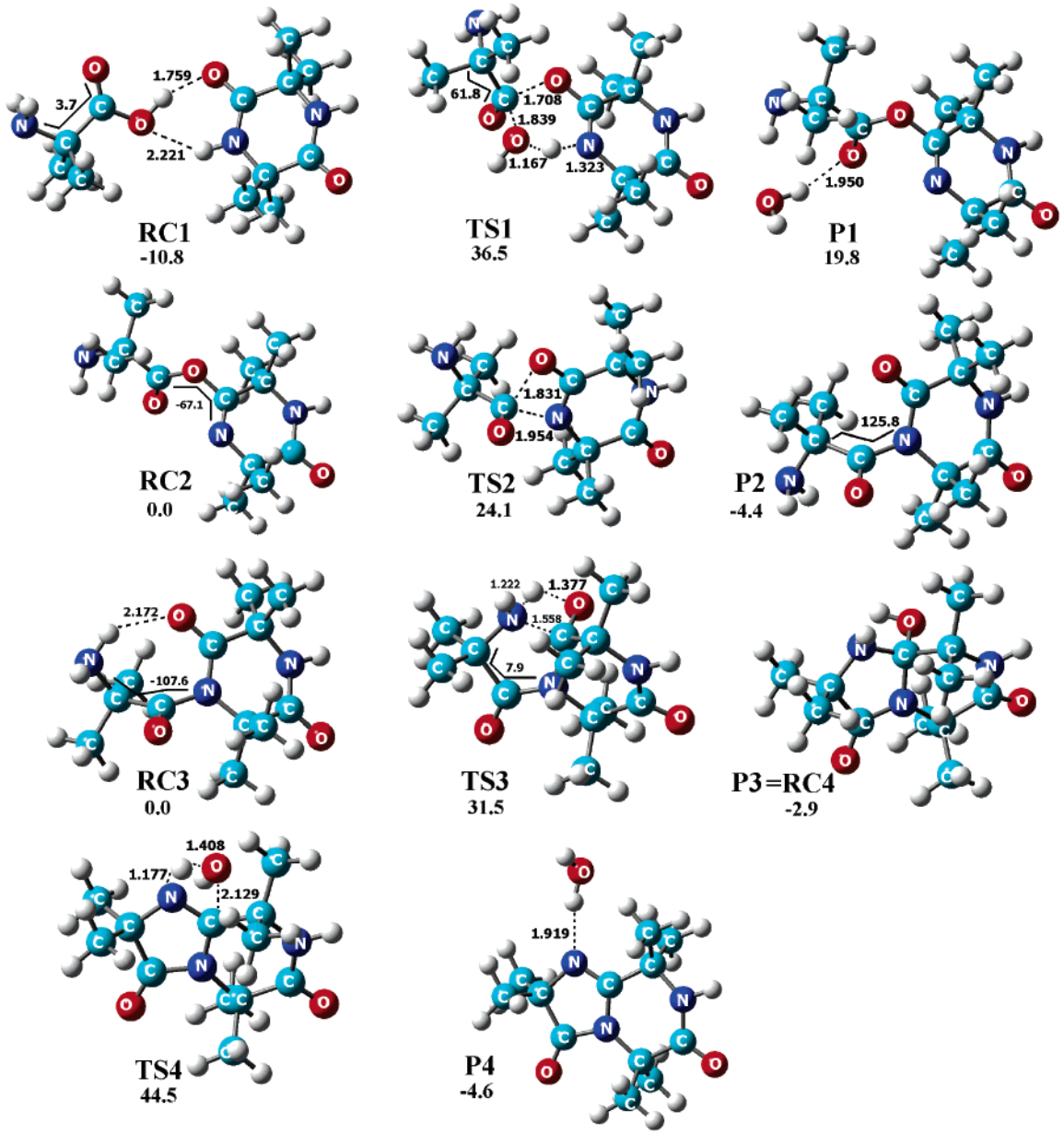

Figure 6. Optimized geometries for reaction complexes (RCs), transition states (TSs) and products (Ps) for the gas-phase formation of BCA derived from AIB, computed at the B3LYP/6-31G(d) level of theory. Selected interatomic distances (in angstroms), dihedral angles (in degrees) and SCF energies (in kcal mol^{-1}) are specified.

descriptors: (1) the HO−C(═O) and SiO−C(═O) bond strength; (2) electrophilicity of the carbonyl and amide C atoms; (3) nucleophilicity of the silanol, hydroxyl and amide O atoms; (4) nucleophilicity of the amide N atoms.

The bond strength depends on the degree of overlap of electronic clouds for neighboring atoms. The elements of the density matrix, P_{tu}, quantify the contribution to electronic energy due to the cross-products of b basis functions χ_s chosen to build molecular orbitals:

$$\phi_i = \sum_{s=1}^{b} c_{si}\chi_s$$

where the elements of the density matrix, P_{tu}, for a closed-shell system are defined as

$$P_{tu} = 2\sum_{j=1}^{n/2}\sum_{r=1}^{b}\sum_{s=1}^{b} c_{tj}^{*}c_{uj}\chi_r^{*}\chi_s \qquad t = 1, 2, ..., b;\ u = 1, 2, ..., b$$

These coefficients for C−O overlap in the HO−C(═O) and SiO−C(═O) bonds for Gly, related surface ester and stationary points in the gas-phase and silica-catalyzed reactions are specified in Table 4. The SCF values obtained at the B3LYP/6-31G(d) and ONIOM2 B3LYP/6-31G(d):UFF levels of theory were refined by single-point calculations with the 6-311++G-(d,p) basis set. Natural atomic charges calculated for the gas-phase reaction with the program NBO Version 3.1[55] at the same theoretical level are listed in Table 5. Unlike Mulliken and other partition schemes, the NBO scheme is not altered by diffuse functions. From the values in Table 4, one can see that the coefficients P_{tu} decrease from Gly and its surface ester to the corresponding products, where the C−O bond of HO−C(═O) and SiO−C(═O) does not exist anymore, and therefore the coefficients P_{tu} are very low and even negative for the gas-phase P1. One can also see that the C−O bond strength in SiO−C(═O) is higher as compared to that in HO−C(═O). This strong amino acid bonding to silica makes the formation of RC1(Si)

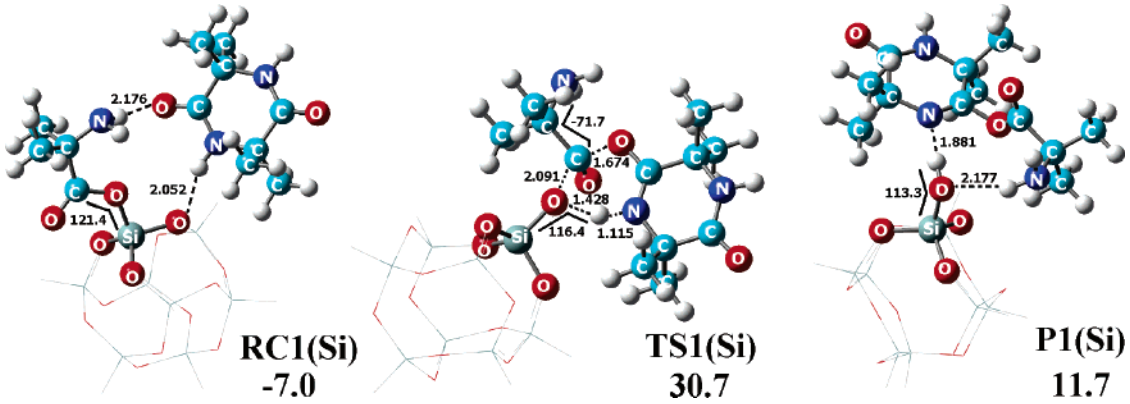

Figure 7. Optimized geometries for reaction complex (RC1(Si)), transition state (TS1(Si)) and product (P1(Si)) for the silica-catalyzed DKP acylation with AIB surface ester, computed at the ONIOM2 B3LYP/6-31G(d):UFF level of theory. The atoms represented by ball-and-stick models were treated with B3LYP/6-31G(d) quantum mechanics; the atoms represented by wire frame models were treated with UFF molecular mechanics. Selected interatomic distances (in angstroms), bond angles, and dihedral angles (in degrees) and SCF energies (in kcal mol^{-1}) are specified.

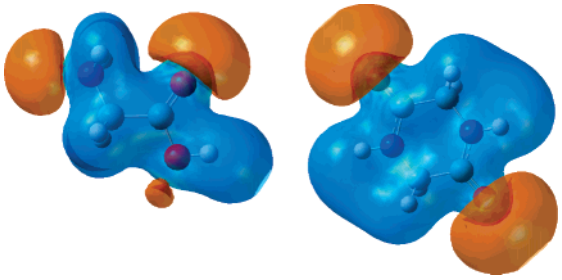

Figure 8. Molecular electrostatic potential isosurfaces (at 0.03 au) for Gly and related DKP. Yellow and blue lobes correspond to negative and positive potential, respectively.

TABLE 3: Gibbs Free Energies at 298 K (in kcal mol^{-1}; Relative to the Reactant Level) for Reaction Complexes (RCs), Transition States (TSs) and Products (Ps) in the Gas-Phase and Silica-Catalyzed O-Acylation of DKPs with Amino Acids and Their Surface Esters, Respectively[a]

reaction	RC	TS	P
Gly gas phase[b]	1.9	49.2	28.2
Gly silica-catalyzed[c]	15.6	51.3	34.1
AIB gas phase[d]	0.3	47.5	30.3
AIB silica-catalyzed[e]	5.2	44.2	25.2

[a] The energies were calculated at the DFT B3LYP/6-31G(d) (gas-phase reactions) and ONIOM2 B3LYP/6-31G(d):UFF (silica-catalyzed reactions; SCF energies) levels of theory. [b] RC1, TS1 and P1 in Figure 3. [c] RC1(Si), TS1(Si) and P1(Si) in Figure 4. [d] RC1, TS1 and P1 in Figure 6. [e] RC1(Si), TS1(Si) and P1(Si) in Figure 7.

TABLE 4: C−O Bond Strength for Gly, Related Surface Ester and Stationary Points in the Gas-Phase and Silica-Catalyzed Reactions, Calculated at the B3LYP/6-311++G(d,p) Level of Theory (Single-point Calculations on the B3LYP/6-31G(d) and ONIOM2 B3LYP/6-31G(d):UFF Geometries)

	coefficents P_{tu}			
	Gly/ester	RC1	TS1	P1
HO−C(=O)	0.464	0.115	−0.195	−0.178
SiO−C(=O)	0.546	0.512	0.099	0.017

endothermic by 1.7 kcal mol^{-1} versus the exothermic one (−8.7 kcal mol^{-1}) for the gas-phase RC1. On the other hand, this gives rise to the catalytic effect by reducing the activation barrier by 9.1 kcal mol^{-1} for the surface reaction.

Although bond overlap density is used as a criterion of the bond strength, natural atomic charges characterize the electrophilicity of carbon atoms and the nucleophilicity of O and N atoms. According to the NBO theory, the change in electronic density as a result of the formation of new chemical species (i.e., RCs, TSs and Ps) can be identified by comparing the atomic charges in reactants. The natural atomic charges for Gly, related DKP and stationary points in the gas-phase O-acylation reaction are listed in Table 5. The values for the C and H atoms in Gly, DKP, RC1, TS1 and P1 (the H atoms in P1 belong to water molecule to be eliminated, and their charges are not relevant anymore) are all positive, whereas all the values for the N and O atoms are negative. In this way, electrophilic properties of the carbon atoms and nucleophilic properties of the oxygen atoms govern the formation of O-acylated products. For example, $C_{carbonyl}$ is more electrophilic in RC1 and TS1 than in Gly, and then its degree of electrophilicity is partially recovered in P1. The electrophilic character of C_{amide} increases from DKP to RC1, and then strongly decreases to P1. The stronger electrophile is obviously $C_{carbonyl}$. Likewise, the nucleophilicity of $O_{hydroxyl}$ considerably increases (by 0.134 charge units) from Gly to TS1, inducing a strong attraction of amide proton H_{amide} resulting in the formation of water molecule in P1. As regards the conversion of C_{amide}−N_{amide} into a double bond, it is seen that N_{amide} reduces its nucleophilic character, first gradually from DKP to TS1 and then dramatically to P1. Finally, from the charge on O_{ester} in P1, one can see how the nucleophilic character of O_{amide} decreased after it became a part of the new ester bond. The preference to form the O-acylated versus N-acylated product can be explained by comparing the charges on O_{amide} and N_{amide} atoms in RC1, which are −0.657 and −0.623, respectively, whereas in free DKP they are −0.620

TABLE 5: Natural Atomic Charges, HOMO and LUMO Energies (in eV) Calculated at the B3LYP/6-311++G(d,p) Level of Theory (Single-point Calculations on the B3LYP/6-31G(d) Geometries) for Gly, Related DKP and Stationary Points in the Gas-Phase O-acylation Reaction

	Gly	DKP	RC1	TS1	P1
$C_{carbonyl}$	0.783		0.805	0.804	0.799
$O_{carbonyl}$	−0.610		−0.603	−0.574	−0.584
$O_{hydroxyl}$	−0.690		−0.747	−0.824	*a*
$H_{hydroxyl}$	0.484		0.515	0.472	*a*
C_{amide}		0.674	0.687	0.667	0.605
O_{amide}		−0.620	−0.657	−0.655	*b*
N_{amide}		−0.633	−0.623	−0.622	−0.498
H_{amide}		0.400	0.423	0.480	*a*
O_{ester}					−0.582[b]
E_{LUMO}	0.17	0.35	−0.18	−0.84	−1.47
E_{HOMO}	−6.79	−6.83	−6.31	−7.19	−6.95

[a] For P1, the charges for $O_{hydroxyl}$, $H_{hydroxyl}$ and H_{amide} are not specified, because these atoms form water molecule. [b] O_{ester} in P1 is formerly O_{amide} in DKP.

and −0.633, respectively. Thus, the charges on O_{amide} and N_{amide} atoms change upon the formation of RC1 by +0.037 and −0.010 units. For comparison, the charges on $C_{carbonyl}$ and $O_{hydroxyl}$ atoms in Gly change by 0.022 and −0.057 units due to the hydrogen bonding in RC1.

The occupation numbers for valence orbitals (VOs) for Gly $C_{carbonyl}$ also change along the reaction coordinate. Natural population analysis showed that no changes can be observed in the Rydberg (Ry) orbitals, whereas all the populations redistribute within VOs. In turn for RC1, the $C_{carbonyl}$, $O_{carbonyl}$ and N_{amide} atoms exhibit no changes in their natural populations (i.e., 2p orbitals). At the same time, changes in the populations of 2s and 2p VOs occur for $O_{hydroxyl}$ and O_{amide}, respectively, which both bear a negative charge. The population changes for $H_{hydroxyl}$ and H_{amide} (whose positive charge increases steadily along the reaction coordinate) are in their 1s VOs. A decrease in the charge density on C_{amide} and N_{amide} in RC1 as compared to DKP is accompanied by a charge transfer from H_{amide} to O_{amide}. The negatively charged atoms O_{amide} and $O_{hydroxyl}$ attract $H_{hydroxyl}$ and H_{amide}, thus forming two hydrogen bridges through their 2p and 2s VOs, respectively. In other words, both amino acid and DKP molecules act simultaneously as electron/proton donors and acceptors. Nevertheless, the above analysis defines the following order for the importance of orbital interactions in H-bonding:

$$O_{2s}\cdots H_{1s} > O_{2p}\cdots H_{1s}$$

In addition, from the frontier orbital energies calculated (Table 5) one can see that the high energy of bonding HOMO (−7.2 eV) in TS1 correlates with the increase of positive charge on $C_{carbonyl}$ and of negative charge on the leaving atom $O_{hydroxyl}$. That is, $C_{carbonyl}$ becomes more electrophilic and, vice versa, $O_{hydroxyl}$ becomes more nucleophilic. At the same time, antibonding LUMO in TS1 with the energy of −0.8 eV reduces the negative charge on N_{amide} making it less nucleophilic toward $C_{carbonyl}$.

The above data demonstrate that our original hypothesis on the DKP acylation mechanism, both in the gas phase and on the silica surface (Scheme 1), was incorrect. Instead of the direct N-acylation, the reaction takes place in two steps: (1) O-acylation, and (2) transfer of the *O*-acyl group (Gly or AIB moiety) to the nitrogen atom. At the same time, the product of O-acylation is the same compound for the gas-phase and surface reaction, and we continue to believe that its further conversion into BCA can occur in the gas phase.

P1 and P1(Si) O-acylation products lose the water molecule and $H_7Si_8O_{12}$−OH cluster, respectively, and thus convert into the same reaction complex RC2 (for Gly, Figure 3; for AIB, Figure 6). The next reaction step is a monomolecular transfer reaction, and therefore, TS2 and P2 energies were calculated relative to the RC2 energy. The barriers separating RC2s and P2s are rather high, 18.9 (Gly TS2) and 24.1 kcal mol^{-1} (AIB TS2). The larger value in the latter case can be explained by steric influence of the geminal CH_3 groups in AIB derivatives. The distances (O)C···O═C are slightly shorter than (O)C···N distances, namely, 1.836 vs 1.938 Å in Gly TS2, and 1.831 vs 1.954 Å in AIB TS2. Finally, the formation energies for Gly P2 and AIB P2 are −16.3 and −4.4 kcal mol^{-1}, respectively. In other words, the transfer reaction is exothermic in both cases but is much more favorable for Gly, whose moieties do not contain bulky α-substituents.

It is the next, third step where the formation of bicyclic system occurs. The reaction complexes here are essentially identical to P2s, with the only difference that the *N*-acyl moiety underwent rotation. (It is unlikely to require high energy, and we did not perform transition state search for this process.) As a result, the dihedral angle N−C−C−N changes from 173.5° in Gly P2 to −87.6° in Gly RC3, and a new weak hydrogen bonding is observed between the NH_2 and C═O groups (Figure 3), with a separation of 2.233 Å. Similarly, the dihedral angle N−C−C−N changes from 125.8° in AIB P2 to −107.6° in AIB RC3 (Figure 6), and the corresponding NH···O═C distance is 2.172 Å. Again, this is a monomolecular process, and therefore TS3 and P3 energies were calculated relative to the RC3 energy. The amino nitrogen atom has to approach the carbonyl carbon atom of the piperazine ring, and the presence of the carbonyl O atom complicates the process. This circumstance explains high energies of Gly TS3 and AIB TS3, of 41.4 and 31.5 kcal mol^{-1}, respectively. At the same time, it is not obvious why the transition state energy in the case of Gly (with no α-substituents) is by ca. 10 kcal mol^{-1} higher as compared to the value for AIB. Both TS3 geometries exhibit typical features with quaternized C atoms, with the transient (H)N···C distance of 1.569 and 1.558 Å for Gly TS3 and AIB TS3, respectively. Both products P3 belong to the class of cyclols,[56,57] in which the formerly carbonyl C atom remains quaternized, being covalently bonded to NH and OH groups. The formation of Gly P3 is slightly endothermic by 3.0 kcal mol^{-1}, whereas the process is exothermic to the same degree (2.9 kcal mol^{-1}) for its AIB counterpart.

The last step necessary for BCA formation is the elimination of water from cyclols. The P3 molecules are rigid, no conformational change is necessary to convert them into RC4 (that is, P3s are totally identical to RC4s; Figures 3 and 6), and therefore we calculated TS4 and P4 energies relative to the level of RC3. Of all the steps studied, this process requires the highest energy: Gly TS4 and AIB TS4 energies are 50.8 and 44.5 kcal mol^{-1}, respectively. Besides that, it again turns to be exothermic for AIB BCA (=AIB P4) contrary to Gly BCA (=Gly P4). Comparing the heats of formation for P3 and P4, one can conclude that the two-step BCA formation from N-acylated DKP is notably less favorable for Gly than for AIB.

4. Conclusions

The entire process of imidazo[1,2-*a*]pyrazine-3,6-dione formation from DKP and a free or silica-bonded (ester-linked) amino acid requires four steps: (1) O-acylation of DKP with the free or silica-bonded amino acid; (2) acyl transfer from the oxygen to the nitrogen atom of DKP ring; (3) intramolecular condensation of the *N*-acyl DKP into a cyclol; (4) the elimination of water molecule. Thus, the mechanism in Scheme 1 suggested earlier is incorrect, because the first step is the O-acylation of DKP, and not N-acylation. The catalytic effect of silica was observed for both Gly and AIB derivatives: the activation energy in the O-acylation at the surface was lower by more than 9 kcal mol^{-1} as compared to the gas-phase process. Contrary to the exothermic O-acylation, the gas-phase transfer reaction (step 2) was exothermic in both cases, being much more favorable for Gly. The cyclocondensation of N-acylated DKPs into BCAs (steps 3 and 4) is endothermic for Gly and exothermic for AIB.

Acknowledgment. We appreciate financial support from UNAM (grant DGAPA-IN100303), Antonio Ramírez Fernández and Martín Cruz Villafañe from the Computer Unit of ICN for technical support. F.F.C.-T. thanks DGEP UNAM for a Ph.D. fellowship.

References and Notes

(1) Basiuk, V. A. *Russ. Chem. Rev.* **1997**, *66*, 187.

(2) Jones, D. S.; Kenner, G. W.; Sheppard, R. C. *Experientia* **1963**, *19*, 126.

(3) Jones, D. S.; Kenner, G. W.; Preston, J.; Sheppard, R. C. *Tetrahedron* **1965**, *21*, 3209.

(4) Titlestad, K. In *Chemistry and Biology of Peptides, The 3rd American Peptide Symposium*; Ann Arbor Science: Ann Arbor, MI, 1972; p 59.

(5) Ali, M. Y.; Dale, J.; Titlestad, K. *Acta Chem. Scand.* **1973**, *27*, 1509.

(6) Ali, M. Y. In *Protein Structure−Function, Proceedings of the International Symposium*; TWEL Publishers: Karachi, 1990; p. 209.

(7) Ali, M. Y.; Khatun, A. *Tetrahedron* **1985**, *41*, 451.

(8) Collins, J. R.; Loew, G. H.; Luke, B. T. *Orig. Life Evol. Biosphere* **1988**, *18*, 107.

(9) Bernal, J. D. *The Physical Basis of Life*; Routledge and Kegan Paul: London, 1951.

(10) Rode, B. M. *Peptides* **1999**, *20*, 773.

(11) Groenewegen, J.; Sachtler, W. *J. Catal.* **1972**, *27*, 369.

(12) Brack, A. *Clay Miner.* **1976**, *11*, 117.

(13) Lahav, N.; White, D.; Chang, S. *Science* **1978**, *201*, 67.

(14) White, D. H.; Erickson, J. C. *J. Mol. Evol.* **1980**, *16*, 279.

(15) Lahav, N.; White, D. H. *J. Mol. Evol.* **1980**, *16*, 11.

(16) Paecht-Horowitz, M.; Eirich, F. R. *Orig. Life Evol. Biosphere* **1988**, *18*, 359.

(17) Fripiat, J. J.; Cloos, P.; Calicis, B.; Makay, K. *Proc. Int. Clay Conf. Jerusalem* **1966**, *1*, 233.

(18) Degens, E. T.; Matheja, J. In *Prebiotic and Biochemical Evolution*; Kimball, A. P., Oró, J., Eds.; North-Holland Publising Co.: Amsterdam, 1970; pp 39−69.

(19) Rohlfing, D. L.; McAlhaney, W. W. *BioSystems* **1976**, *8*, 139.

(20) White, D. H.; Kennedy, R. M.; Macklin, J. *Orig. Life Evol. Biosphere* **1984**, *14*, 273.

(21) Budják, J.; Rode, B. M., *React. Kinet. Catl. Lett.* **1997**, *62*, 281.

(22) Budják, J.; Rode, B. M. *J. Mol. Evol.* **1997**, *45*, 457

(23) Meng, M.; Stievano, L.; Lambert, J.-F. *Langmuir* **2004**, *20*, 914.

(24) Basiuk, V. A.; Gromovoy, T. Yu.; Golovaty, V. G.; Glukhoy, A. M. *Orig. Life Evol. Biosphere* **1991**, *20*, 483.

(25) Basiuk, V. A.; Gromovoy, T. Yu.; Chuiko, A. A.; Soloshonok, V. A.; Kukhar, V. P. *Synthesis* **1992**, No. 5, 449.

(26) Basiuk, V. A.; Gromovoy, T. Yu.; Glukhoy, A. M.; Golovaty, V. G. *Orig. Life Evol. Biosphere* **1991**, *21*, 129.

(27) Gromovoy, T. Yu.; Basiuk, V. A.; Chuiko, A. A. *Orig. Life Evol. Biosphere* **1991**, *21*, 119.

(28) Basiuk, V. A. *Orig. Life Evol. Biosphere* **1992**, *22*, 333.

(29) Young, R. P. *Can. J. Chem.* **1969**, *47*, 2237.

(30) Macklin, J. W.; White, D. H. *Spectrochim. Acta A* **1985**, *41*, 851.

(31) (a) Basiuk, V. A.; Navarro-González, R.; Basiuk, E. V. *J. Anal. Appl. Pyrol.* **1998**, *45*, 89. (b) Basiuk, V. A. *J. Anal. Appl. Pyrol.* **1998**, *47*, 127.

(32) Basiuk, V. A.; Navarro-González, R *Icarus*, **1998**, *134*, 269.

(33) Simmonds, P.; Medley, E.; Ratcliff, A.; Shulman, G. *Anal. Chem.* **1972**, *44*, 2060.

(34) Ratcliff, M.; Medley, E.; Simmonds, P. *J. Org. Chem.* **1974**, *39*, 1481.

(35) Basiuk, V. A.; Navarro-González, R. *J. Chromatogr. A* **1997**, *776*, 255.

(36) Basiuk, V. A.; Van Meervelt, L.; Soloshonok, V. A.; Basiuk, E. V. *Acta Crystallogr. C* **2000**, *56*, 598.

(37) Rimola, A.; Tosoni, S.; Sodupe, M.; Ugliengo, P. *Chem. Phys. Lett.* **2005**, *408*, 295.

(38) Lomenech, C.; Bery, G.; Costa, D.; Stievano, L.; Lambert, J.-F. *Chem. Phys. Chem.* **2005**, *6*, 1061.

(39) Rimola, A.; Tosoni, S.; Sodupe, M.; Ugliengo, P. *Chem. Phys. Chem* **2006**, *7*, 157.

(40) Sauer, J.; Hill, J.-R. *Chem. Phys. Lett.* **1994**, *218*, 333.

(41) Civalleri, B.; Garrone, E.; Ugliengo, P. *Chem. Phys. Lett.* **1998**, *294*, 103.

(42) Civalleri, B.; Garrone, E.; Ugliengo, P. *Chem. Phys. Lett.* **1999**, *443*, 299.

(43) Civalleri, B.; Garrone, E.; Ugliengo, P. *Langmuir* **1999**, *15*, 5829.

(44) Roggero, I.; Civalleri, B.; Ugliengo, P. *Chem. Phys. Lett.* **2001**, *341*, 625.

(45) Frisch, M. J.; Trucks, G. W.; Schlegel, H. B.; Scuseria, G. E.; Robb, M. A.; Cheeseman, J. R.; Montgomery, J. A., Jr.; Vreven, T.; Kudin, K. N.; Burant, J. C.; Millam, J. M.; Iyengar, S. S.; Tomasi, J.; Barone, V.; Mennucci, B.; Cossi, M.; Scalmani, G.; Rega, N.; Petersson, G. A.; Nakatsuji, H.; Hada, M.; Ehara, M.; Toyota, K.; Fukuda, R.; Hasegawa, J.; Ishida, M.; Nakajima, T.; Honda, Y.; Kitao, O.; Nakai, H.; Klene, M.; Li, X.; Knox, J. E.; Hratchian, H. P.; Cross, J. B.; Adamo, C.; Jaramillo, J.; Gomperts, R.; Stratmann, R. E.; Yazyev, O.; Austin, A. J.; Cammi, R.; Pomelli, C.; Ochterski, J. W.; Ayala, P. Y.; Morokuma, K.; Voth, G. A.; Salvador, P.; Dannenberg, J. J.; Zakrzewski, V. G.; Dapprich, S.; Daniels, A. D.; Strain, M. C.; Farkas, O.; Malick, D. K.; Rabuck, A. D.; Raghavachari, K.; Foresman, J. B.; Ortiz, J. V.; Cui, Q.; Baboul, A. G.; Clifford, S.; Cioslowski, J.; Stefanov, B. B.; Liu, G.; Liashenko, A.; Piskorz, P.; Komaromi, I.; Martin, R. L.; Fox, D. J.; Keith, T.; Al-Laham, M. A.; Peng, C. Y.; Nanayakkara, A.; Challacombe, M.; Gill, P. M. W.; Johnson, B.; Chen, W.; Wong, M. W.; Gonzalez, C.; Pople, J. A. *Gaussian 03W*, revision B.04; Gaussian, Inc.: Pittsburgh, PA, 2003.

(46) Maseras, F.; Morokuma, K. *J. Comput. Chem.* **1995**, *16*, 1170.

(47) Vreven, T.; Morokuma, K.; Farkas, Ö.; Schlegel, H. B.; Frisch, M. J. *J. Comput. Chem.* **2003**, *24*, 760.

(48) Rappé, A. K.; Casewit, C. J.; Colwell, K. S.; Goddard, W. A., III; Skiff, W. M. *J. Am. Chem. Soc.* **1992**, *114*, 10024.

(49) Becke, A. D. *J. Chem. Phys.* **1993**, *98*, 5648.

(50) Lee, C.; Yang, W.; Parr, R. G. *Phys. Rev. B* **1988**, *37*, 785.

(51) Binkley, J. S.; Pople, J. A.; Hehre, W. J. *J. Am. Chem. Soc.* **1980**, *102*, 939.

(52) Hariharan, P. C.; Pople, J. A. *Chem. Phys. Lett.* **1972**, *66*, 217.

(53) Contreras-Torres, F. F.; Basiuk, V. A. *Spectrochim. Acta A* **2005**, *61*, 2560.

(54) Simons, J.; Jørgensen, P.; Taylor, H.; Ozment, J. *J. Phys. Chem.* **1983**, *87*, 2745.

(55) Glendening, E. D.; Reed, A. E.; Carpenter, J. E.; Weinhold, F. NBO Version 3.1.

(56) Lucente, G.; Pinnen, F.; Romeo, A.; Zanotti, G. *J. Chem. Soc., Perkin Trans.* **1983**, *1*, 1127.

(57) Zanotti, G.; Pinnen, F.; Lucente, G.; Cerrini, S.; Gavazzo, E.; Mazza, F. *Int. J. Pept. Protein Res.* **1983**, 410.